

Supplementary Information for

Nitrogen and Oxygen Tailoring Solid Carbon Active Site for Two-electron Selectivity Electrocatalysis

Hongyang Shao,^{a†} Quan Zhuang,^{a†} Hongda Gao,^b Yin Wang,^{*a} Lei Ji,^a Xia Wang,^a Tingting Zhang,^{*a} Limei Duan,^a Jie Bai,^b Zhiqiang Niu,^c and Jinghai Liu^{*a}

^a. *Inner Mongolia Key Laboratory of Carbon Nanomaterials, Nano Innovation Institute (NII), College of Chemistry and Materials Science, Inner Mongolia University for Nationalities Tongliao 028000, People's Republic of China.*

*E-mail: jhliu2008@sinano.ac.cn; wy19890703@126.com; duanlmxie@126.com

^b. *Chemical Engineering College, Inner Mongolia University of Technology, Huhhot 010051, People's Republic of China.*

^c. *Key Laboratory of Advanced Energy Materials Chemistry (Ministry of Education), Renewable Energy Conversion and Storage Center, College of Chemistry, Nankai University, Tianjin 300071, People's Republic of China.*

†These authors contributed equally to this work.

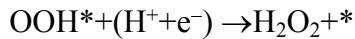
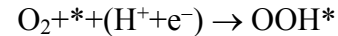
*Corresponding author.

Contents

Supplementary Computational details	S3
Supplementary Tables.....	S4
Proportion for bonding configurations of carbon atoms	S4
Electrocatalysts summarization.....	S5
Supplementary Figures	S6
Free energy diagrams	S6
Polarization curves.....	S7
SEM images.....	S8
XRD patterns	S9
Raman spectra.....	S10
XPS survey	S11
High-resolution C 1s peaks of XPS survey.....	S12
Calibration curve of H ₂ O ₂ concentration	S13
Supplementary References.....	S14

Supplementary Computational details

The two-electron ORR pathway can be summarized as¹:



in which, * represents the adsorption site. The reaction free energies of reactants and each intermediate state were estimated by applying zero-point energy and entropic corrections to the calculated DFT energies using the equation:

$$\Delta G = \Delta E + \Delta ZPE - T\Delta S - neU$$

where ΔE , ΔZPE and ΔS represent the differences in the calculated DFT energies, zero-point energy and entropy of the reaction, respectively. The electrode potential was taken into account by shifting the electron energy by $-neU$, where n is the electron number of such state, e is the elementary charge, and U is the potential at the electrode. Since the ground states of the oxygen and H_2O_2 molecules are poorly described in DFT calculations, we have adopted the gas-phase H_2O and hydrogen as reference states which are readily treated in the DFT calculations. The energy corrections of ΔZPE and ΔS were analyzed by using VASPKIT program².

Supplementary Tables

Proportion for bonding configurations of carbon atoms

Table S1. Proportion (at.%) for bonding configurations of carbon atoms for all catalysts determined by XPS.

Sample	C1s Bonding Types (at.%)			
	C-C	C-N	C-O	O-C=C/N-C=N
CNO-glu	62.16	16.05	15	6.79
CNO- glu-H	62.43	21.17	10.41	5.98
CNO-cyc	63.06	15.25	13.46	8.31
CNO-cyc-H	62.04	20.62	10.55	6.78
CNO-cel	72.06	12.02	10.16	5.76
CNO- cel-H	64.42	19.18	9.85	6.55

Electrocatalysts summarization

Table S2. Summarization of 2e⁻ ORR performance for different electrocatalysts.

Electrocatalysts	electrolyte	H ₂ O ₂ production rate	H ₂ O ₂ selectivity	References
Mesoporous Nitrogen-Doped Carbon	0.1M HClO ₄	-	-	[3]
N-doped porous carbons	0.1M KOH	-	93%	[4]
Mesoporous Nitrogen-Doped Carbon	0.5M H ₂ SO ₄	-	>90%	[5]
Nitrogen-doped mesoporous carbon	0.5M H ₂ SO ₄	561.7 mmol g _{cat} ⁻¹ h ⁻¹	>95%	[6]
Nitrogen-Doped Porous Carbon	0.5M H ₂ SO ₄	570 mmol g _{cat} ⁻¹ h ⁻¹	95%	[7]
BN-C	0.1M KOH	-	90%	[8]
O-CNTs	0.1M KOH	1,975 mg L ⁻¹ within 30 min	>90%	[9]
O-GOMC	0.1M KOH	-	>90%	[10]
OCB	0.1M KOH	-	>60%	[11]
NT-3DFG	0.1M KOH	-	>90%	[12]
Mesoporous defective carbon	0.1M KOH	-	80%	[13]
oxo-G	0.1M KOH	224.8 mmol g _{cat} ⁻¹ h ⁻¹	>82%	[14]
rGO-PEI	0.1M KOH	106 mmol g _{cat} ⁻¹ h ⁻¹	90%	[15]
CMK-3	0.1M KOH	-	90%	[16]
CNO-glu-H	0.1M KOH	214 mmol g _{cat} ⁻¹ h ⁻¹	82%	This work

Supplementary Figures

Free energy diagrams

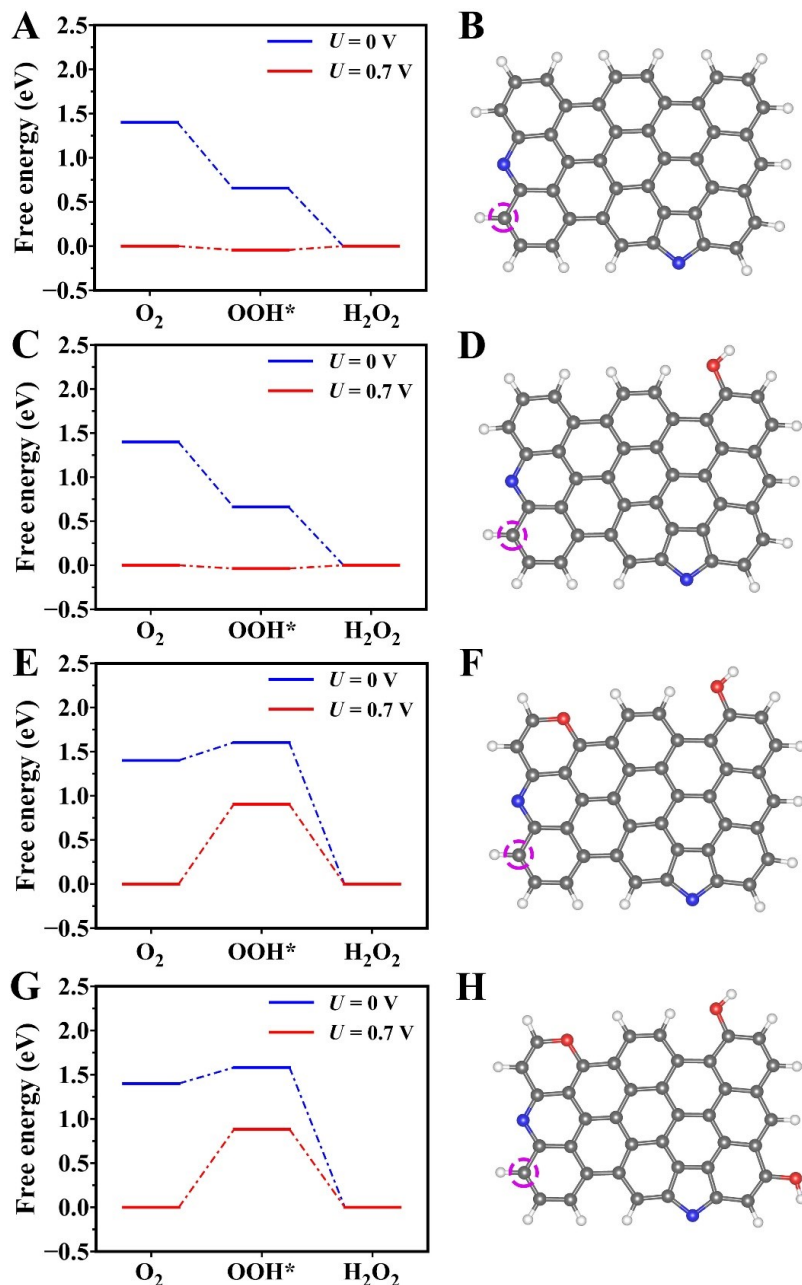


Fig. S1. (A, C, E, G) Free energy diagrams of the oxygen reduction reaction to hydrogen peroxide on different model systems at 0 V and 0.7 V versus RHE. The carbon-based topological structures relevant to the energy profiles are given in the right side and marked as (B, D, F, H), respectively. Color code: C, gray; N, blue; O, red; H, white. The carbon atoms denoted by a dashed magenta circle are the active sites under investigation.

Polarization curves

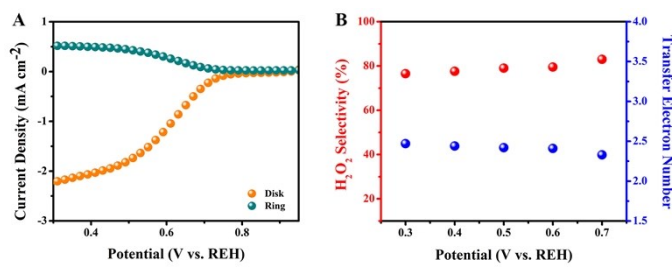


Fig. S2 (A) Polarization curves (orange line) and simultaneous H₂O₂ detection currents at the ring electrode (cyan line) for CNO-glu-H in O₂-saturated 0.1 M KOH solution at 1600 rpm with Hg/HgO reference electrode. **(B)** H₂O₂ selectivity and transfer electron number for CNO-glu-H.

SEM images

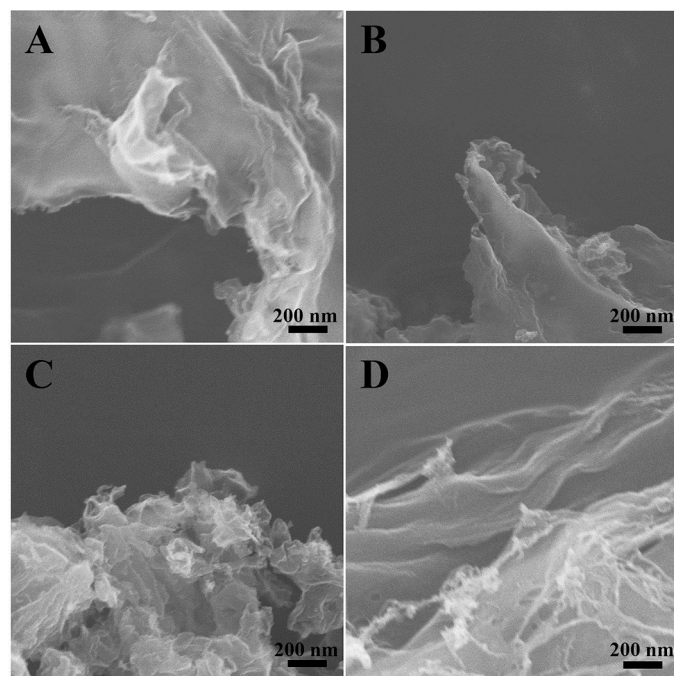


Fig. S3 SEM images of (A) CNO-cyc, (B) CNO-cyc-H, (C) CNO-cel and (D) CNO-cel-H.

XRD patterns

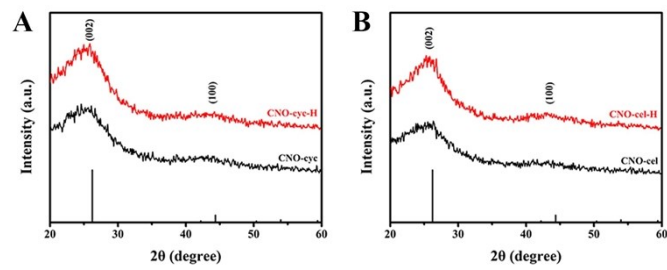


Fig. S4 XRD patterns of (A) CNO-cyc and CNO-cyc-H, (B) CNO-cel and CNO-cel-H.

Raman spectra

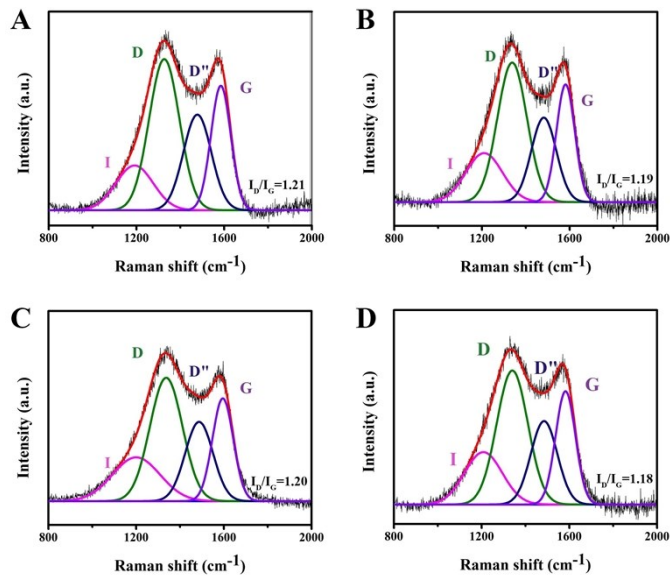


Fig. S5 Raman spectra of (A) CNO-cyc, (B) CNO-cyc-H, (C) CNO-cel and (D) CNO-cel-H.

XPS survey

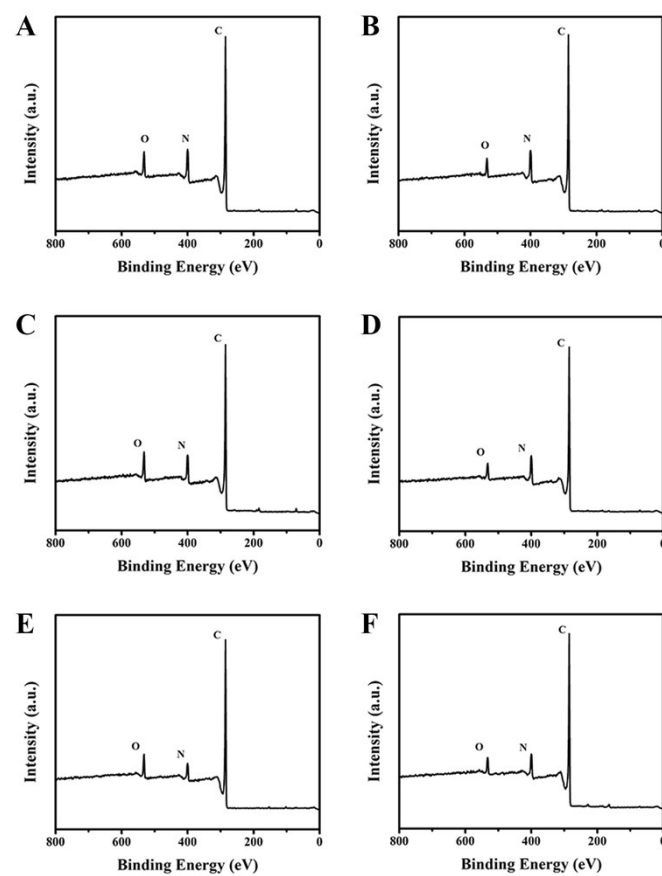


Fig. S6 XPS survey of (A) CNO-glu, (B) CNO-glu-H, (C) CNO-cyc, (D) CNO-cyc-H, (E) CNO-cel, and (F) CNO-cel-H.

High-resolution C 1s peaks of XPS survey

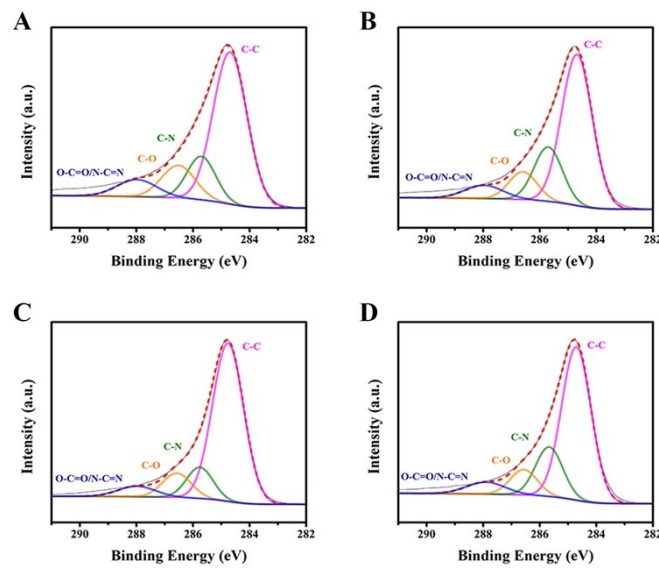


Fig. S7 High-resolution C 1s peaks of (A) CNO-cyc, (B) CNO-cyc-H, (C) CNO-cel, and (D) CNO-cel-H.

Calibration curve of H₂O₂ concentration

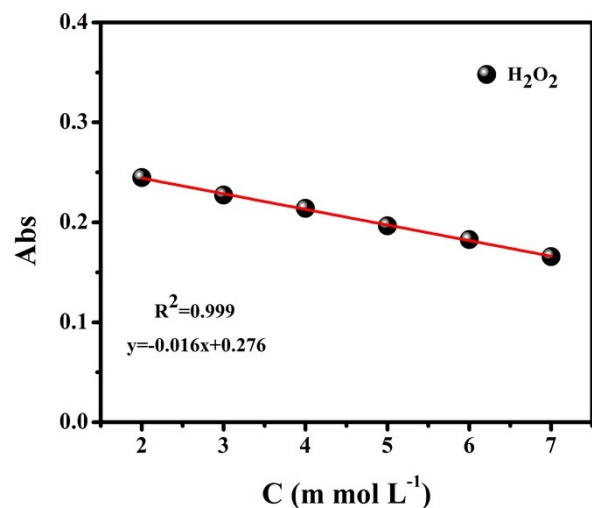


Fig. S8 The calibration curve of H₂O₂ concentration.

Supplementary References:

1. V. Viswanathan, H. A. Hansen, J. Rossmeisl and J. K. Nørskov, Unifying the 2e⁻ and 4e⁻ Reduction of Oxygen on Metal Surfaces, *J. Phys. Chem. Lett.* 2012, **3**, 2948–2951.
2. V. Wang, N. Xu, J.C. Liu, G. Tang and W. T. Geng, VASPKIT: A Pre- and Post-Processing Program for VASP code, 2019, arXiv:1908.08269.
3. T. P. Fellinger, F. Hasche, P. Strasser and M. Antonietti, Mesoporous nitrogen-doped carbon for the electrocatalytic synthesis of hydrogen peroxide, *J Am. Chem. Soc.*, 2012, **134**, 4072-4075.
4. Y.H. Lee, F. Li, K.H. Chang, C.C. Hu and T. Ohsaka, Novel synthesis of N-doped porous carbons from collagen for electrocatalytic production of H₂O₂, *Applied Catalysis B: Environmental*, 2012, **126**, 208-214.
5. J. Park, Y. Nabae, T. Hayakawa and M.a. Kakimoto, Highly Selective Two-Electron Oxygen Reduction Catalyzed by Mesoporous Nitrogen-Doped Carbon, *ACS Catal.*, 2014, **4**, 3749-3754.
6. Y. Sun, I. Sinev, W. Ju, A. Bergmann, S. Dresp, S. Kühl, C. Spöri, H. Schmies, H. Wang, D. Bernsmeier, B. Paul, R. Schmack, R. Kraehnert, B. Roldan Cuenya and P. Strasser, Efficient Electrochemical Hydrogen Peroxide Production from Molecular Oxygen on Nitrogen-Doped Mesoporous Carbon Catalysts, *ACS Catal.*, 2018, **8**, 2844-2856.
7. Y. Sun, S. Li, Z. P. Jovanov, D. Bernsmeier, H. Wang, B. Paul, X. Wang, S. Kuhl and P. Strasser, Structure, Activity, and Faradaic Efficiency of Nitrogen-Doped Porous Carbon Catalysts for Direct Electrochemical Hydrogen Peroxide Production, *ChemSusChem*, 2018, **11**, 3388-3395.
8. S. Chen, Z. Chen, S. Siahrostami, D. Higgins, D. Nordlund, D. Sokaras, T. R. Kim, Y. Liu, X. Yan, E. Nilsson, R. Sinclair, J. K. Norskov, T. F. Jaramillo and Z. Bao, Designing Boron Nitride Islands in Carbon Materials for Efficient Electrochemical Synthesis of Hydrogen Peroxide, *J Am. Chem. Soc.*, 2018, **140**, 7851-7859.

9. Z. Lu, G. Chen, S. Siahrostami, Z. Chen, K. Liu, J. Xie, L. Liao, T. Wu, D. Lin, Y. Liu, T. F. Jaramillo, J. K. Nørskov and Y. Cui, High-efficiency oxygen reduction to hydrogen peroxide catalysed by oxidized carbon materials, *Nature Catal.*, 2018, **1**, 156-162.
10. Y. J. Sa, J. H. Kim and S. H. Joo, Active Edge-Site-Rich Carbon Nanocatalysts with Enhanced Electron Transfer for Efficient Electrochemical Hydrogen Peroxide Production, *Angew Chem. Int. Ed.*, 2019, **58**, 1100-1105.
11. K.H. Wu, D. Wang, X. Lu, X. Zhang, Z. Xie, Y. Liu, B.J. Su, J.M. Chen, D.S. Su, W. Qi and S. Guo, Highly Selective Hydrogen Peroxide Electrosynthesis on Carbon: In Situ Interface Engineering with Surfactants, *Chem.*, 2020, **6**, 1443-1458.
12. D. Roman, D. Krishnamurthy, R. Garg, N. Nuhfer, V. Viswanathan and T. Cohen-Karni, Engineering Three-Dimensional (3D) Out-of-Plane Graphene Edge Sites for Highly-Selective Two-Electron Oxygen Reduction Electrocatalysis, *ACS Catal.* 2020, **10**, 1993–2008.
13. S. Chen, Z. Chen, S. Siahrostami, T. R. Kim, D. Nordlund, D. Sokaras, S. Nowak, J. W. F. To, D. Higgins, R. Sinclair, J. K. Nørskov, T. F. Jaramillo and Z. Bao, Defective Carbon-Based Materials for the Electrochemical Synthesis of Hydrogen Peroxide, *ACS Sustainable Chem. Eng.*, 2017, **6**, 311-317.
14. L. Han, Y. Sun, S. Li, C. Cheng, C. E. Halbig, P. Feicht, J. L. Hübner, P. Strasser and S. Eigler, In-Plane Carbon Lattice-Defect Regulating Electrochemical Oxygen Reduction to Hydrogen Peroxide Production over Nitrogen-Doped Graphene, *ACS Catal.*, 2019, **9**, 1283-1288.
15. X. Xiao, T. Wang, J. Bai, F. Li, T. Ma and Y. Chen, Enhancing the Selectivity of H_2O_2 Electrogeneration by Steric Hindrance Effect, *ACS Appl. Mater. Interfaces*, 2018, **10**, 42534-42541.
16. Z. Chen, S. Chen, S. Siahrostami, P. Chakthranont, C. Hahn, D. Nordlund, S. Dimosthenis, J. K. Nørskov, Z. Bao and T. F. Jaramillo, Development of a reactor with carbon catalysts for modular-scale, low-cost electrochemical generation of H_2O_2 , *React. Chem. Eng.*, 2017, **2**, 239-245.